Supporting Information

Enhancing zinc anode stability *via* dual-additive electrolyte engineering

Jiaming Li[ab], Junyi Han[ab], Nan Li[ab], Changfu Ma[c], Yini Long[ab], Jiaqi Li[ab], Xiao Yu[ab], Jianglin Wang[ab], Zhanhong Yang*[a] Xiaowei Liu*[c]

[a] Hunan Province Key Laboratory of Chemical Power Source, College of Chemistry and Chemical Engineering, Central South University, Changsha, 410083, China.

[b] Innovation Base of Energy and Chemical Materials for Graduate Students Training, Central South University, Changsha, 410083, China.

[C] Chaowei Power Group Co. LTD, PR China

*Corresponding author email-address: zhyangcsu611@163.com (Z. Yang), liuxw888@126.com (X. Liu)

Experimental Section

Preparation of Electrolytes

All aqueous electrolytes were prepared using deionized water as the solvent. First, $ZnSO_4 \cdot 7H_2O$ (Aladdin) was dissolved in deionized water to prepare 2 M $ZnSO_4$ as the baseline electrolyte (BE). Then, different molar amounts of NADH and KI were separately added to the 2 M $ZnSO_4$ solution, followed by stirring at 500 rpm for 6 h to ensure complete dissolution and uniform mixing, thus obtaining the additive-containing electrolytes. Finally, the following electrolytes were prepared: 2 M $ZnSO_4$ (BE), 2 M $ZnSO_4$ + 5 mM NADH (5-N), 2 M $ZnSO_4$ + 10 mM KI (10-K), and 2 M $ZnSO_4$ + 5 mM NADH + 10 mM KI (NK).

Materials Characterizations

Field emission scanning electron microscopy (FESEM, ZEISS Sigma 300, 10 kV) was used to observe the surface morphology of zinc metal after immersion, deposition, and cycling. X-ray diffraction (XRD) characterization was conducted using Cu Kα radiation, with a scanning range of 5-90 ° and a scanning speed of 10 ° min^{-1}. X-ray photoelectron spectroscopy (XPS) measurements were performed on a Thermo ESCALAB 250XI spectrometer, using the C 1*s* peak (284.8 eV) as a calibration reference. Fourier transform infrared spectroscopy (FTIR, Thermo Scientific Nicolet iS20) was used to analyze the molecular vibration states of different electrolytes. Zeta potential measurements were carried out using a Malvern Zetasizer Nano ZS90, while the wettability of the electrolyte on zinc metal was tested using a LAUDA Scientific GmbH LSA-100 instrument. The surface roughness of the anode after cycling was evaluated using an optical profilometer (Bruker Contour GT K 3D). Additionally, an optical microscope (SOPTOP DMSZ7) was used to observe the morphological changes of the zinc anode during deposition.

Electrochemical measurements

The LSV curves were obtained using Zn//Ti batteries within the voltage ranges of

0.5 V to -0.4 V and 2 V to 2.8 V (*vs.* Zn/Zn^{2+}). In the Zn//Zn batteries, the CA curve was recorded at a fixed overpotential of -150 mV. The EIS measurements for Zn//Zn batteries and Zn//AC ZICs were conducted over a frequency range of 0.1 Hz to 100 kHz. The Tafel polarization curves were tested in a three-electrode system, where Zn foil served as the working electrode, Ti foil as the counter electrode, and Ag/AgCl as the reference electrode, with a scan rate of 5 mV s^{-1}. The distribution of relaxation times (DRT) analysis was performed using a Zn//Zn symmetric batteries, where *in-situ* EIS data were recorded every 10 min during the discharge/charge cycles at 0.5 mA·cm^{-2}. Symmetric batteries, Zn//Cu half-batteries, and ZICs were tested using CR2025 coin batteries, with a glass fiber membrane (Whatman GF-D) as the separator. The charge/discharge tests were conducted using a Neware battery testing system. For ZIC assembly, the cathode was composed of 70% active material powder, 20% Super P conductive agent and 10% PVDF binder, coated onto a carbon cloth substrate.

Density functional theory (DFT) calculations

The density functional theory (DFT) calculations were carried out with the VASP code. The Perdew-Burke-Ernzerhof (PBE) functional within generalized gradient approximation (GGA) was used to process the exchange-correlation, while the projectoraugmented-wave pseudopotential (PAW) was applied with a kinetic energy cut-off of 520 eV, which was utilized to describe the expansion of the electronic eigenfunctions. The vacuum thickness was set to be 20 Å to minimize interlayer interactions. For Brillouin zone integration, the Γ-point was considered in the geometry optimizations while otherwise a 4 × 4 × 1 Monkhorst-Pack *k*-grid is used. All atomic positions were fully relaxed until energy and force reached a tolerance of 1×10^{-6} eV and 0.02 eV/Å, respectively. The dispersion corrected DFT-D3 method was employed to consider the long-range interactions. The adsorption energy is calculated *via*:

$$E_{ads} = E_{Zn+mol} - E_{Zn} - E_{mol}$$

where the E_{Zn+mol}, the E_{Zn}, and the E_{mol} represent the total energy of adsorbates on the Zn surface, the energy of the Zn surface, and the energy of the isolated adsorbates,

respectively.

DRT analysis

Distribution of relaxation times (DRT) from the EIS data were calculated by MATLAB R2023b with a toolbox of DRT-TOOLS developed by the research group of Professor Francesco Ciucci. DRT-TOOLS is freely available from the following site: https://github.com/ciuccislab.

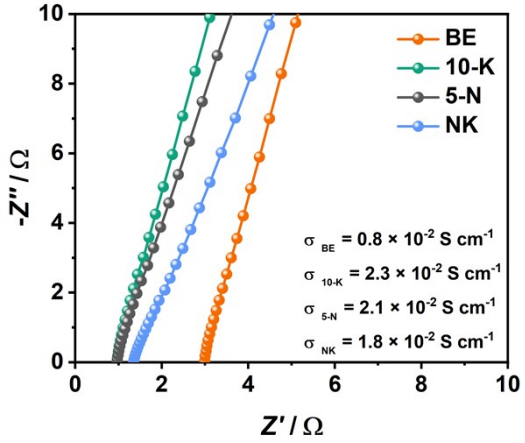

Fig. S1 EIS measurements of different electrolytes for determining the ionic conductivities.

Using two steel plates as blocking electrodes, the ionic conductivity of the electrolyte was tested. The formula for calculating ionic conductivity is as follows:

$$\sigma = \frac{L}{S \cdot R}$$

Where L is the distance between two electrodes, S is the electrode area, and R is the resistance obtained from EIS fitting.

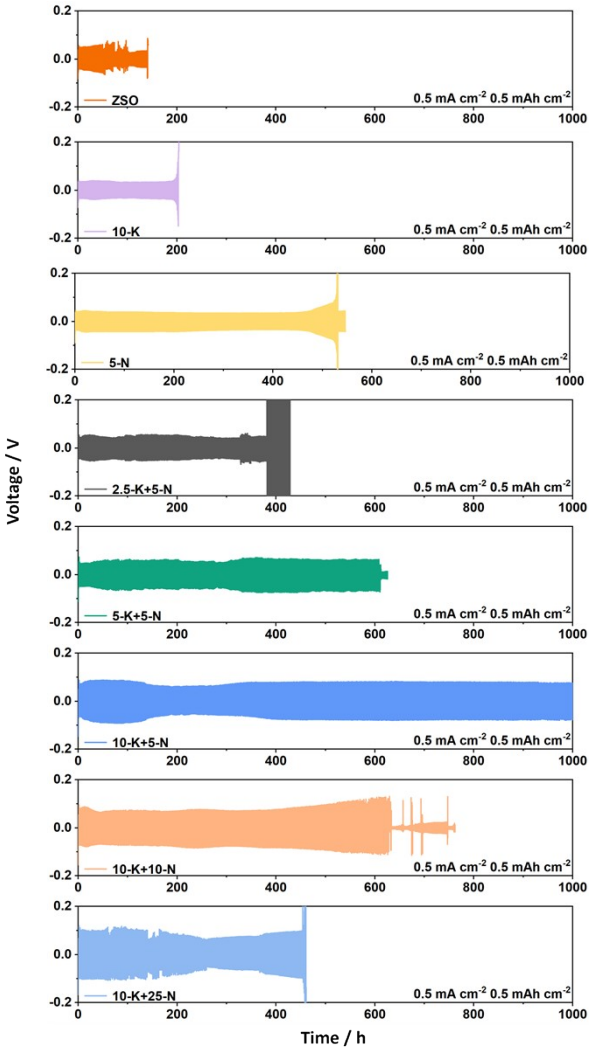

Fig. S2 Cycling tests of symmetric batteries assembled with different additive concentrations.

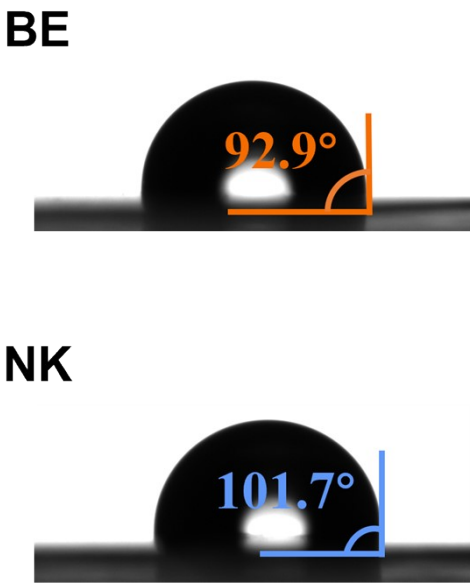

Fig. S3 Contact angle measurements of zinc metal with BE and NK electrolytes.

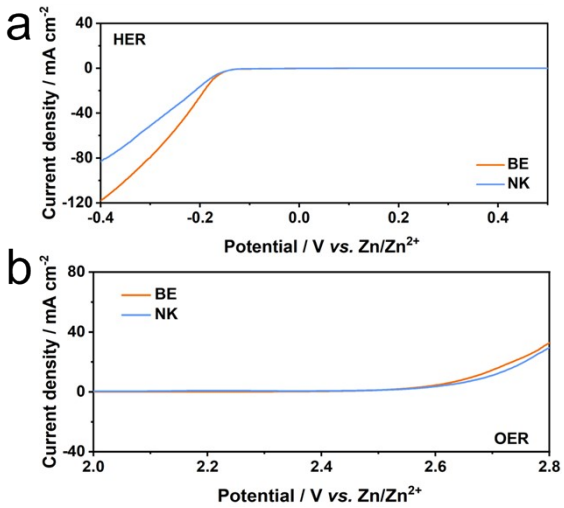

Fig. S4 Linear sweep voltammetry (LSV) curves of BE and NK electrolytes.

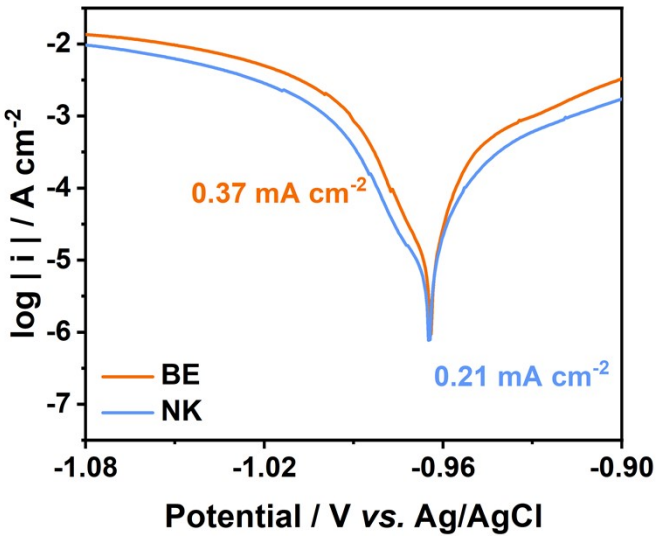

Fig. S5 Linear polarization curves curves of BE and NK.

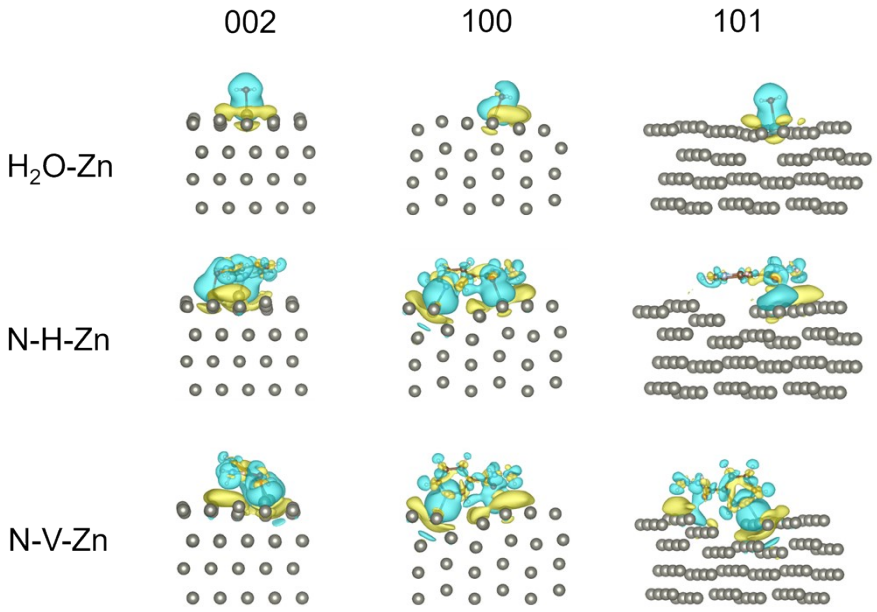

Fig. S6 Electron density of the H_2O-Zn and NADH-Zn.

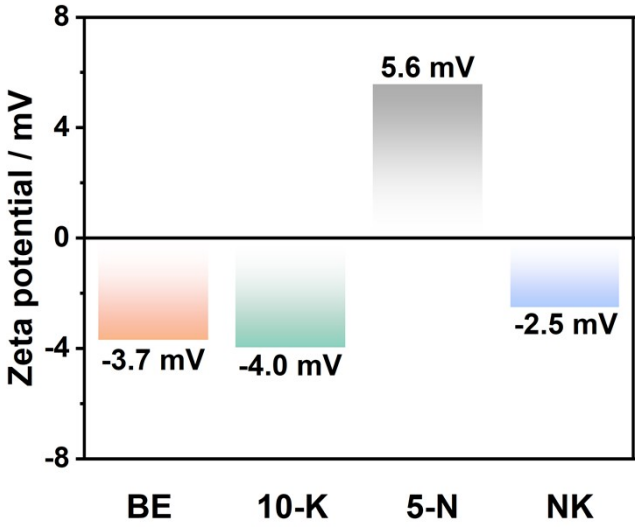

Fig. S7 Zeta potential tests for different electrolytes.

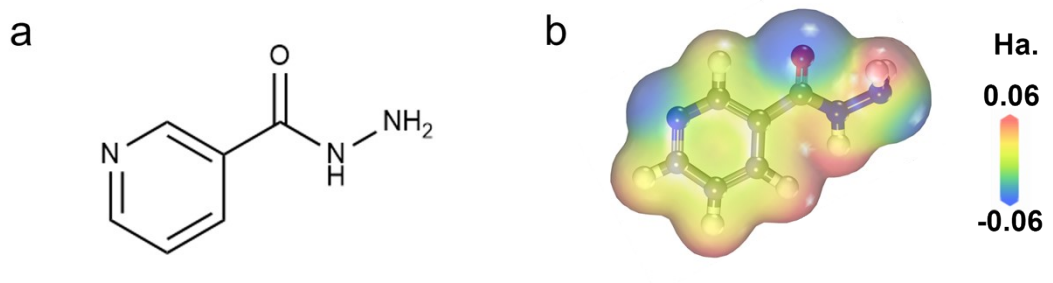

Fig. S8 (a) Molecular structure of NADH and the corresponding (b) electrostatic potential distribution map.

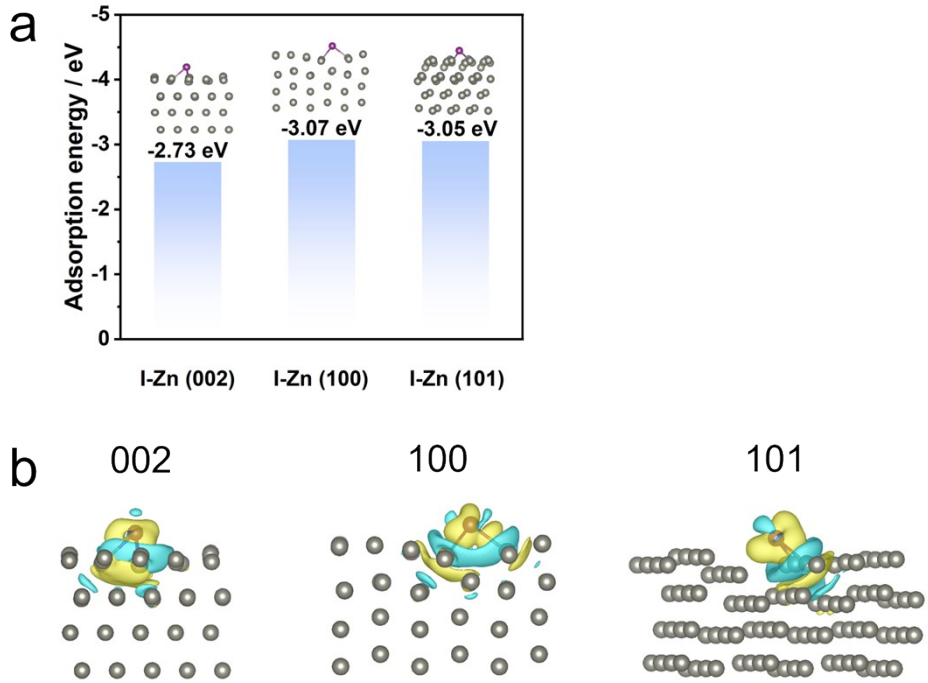

Fig. S9 (a) Adsorption energy of I^- on different zinc metal crystal planes and the corresponding (b) charge density.

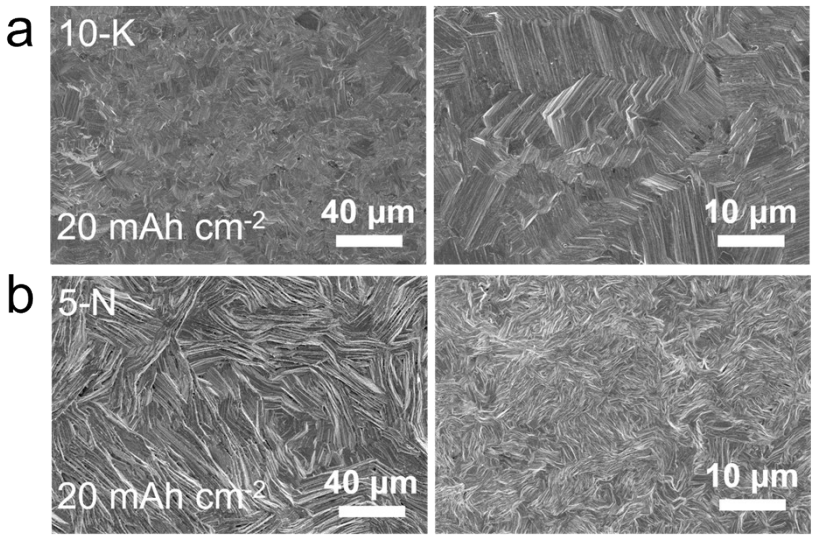

Fig. S10 SEM images of zinc deposition (20 mAh cm^{-2}) on Cu using (a) 10-K and (b) 5-N electrolytes.

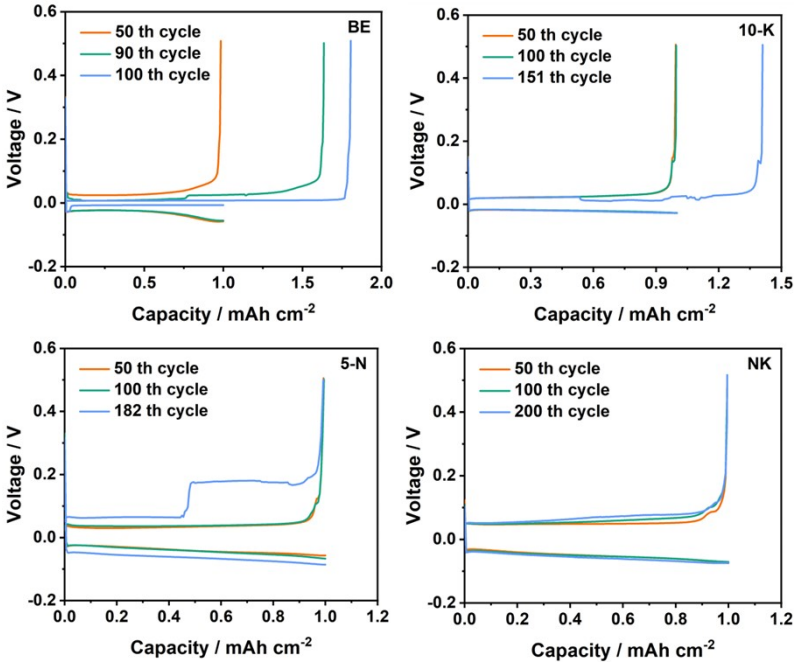

Fig. S11 Charge-discharge curves of Zn//Cu half batteries at different cycle numbers.

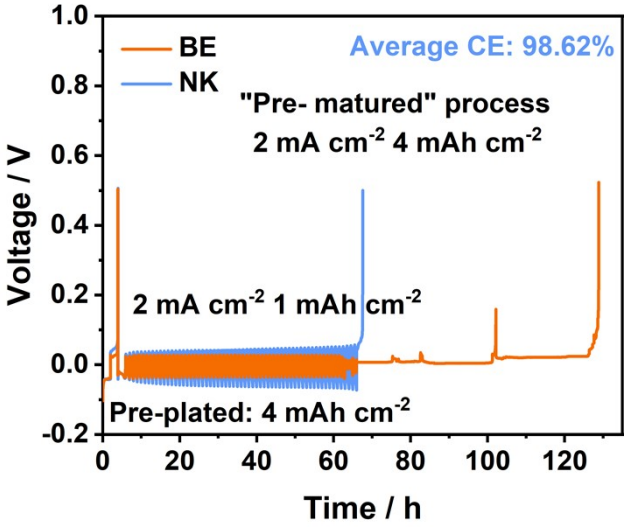

Fig. S12 Zinc plating/stripping CE measurement of Zn//Cu batteries with the "reservoir" protocol.

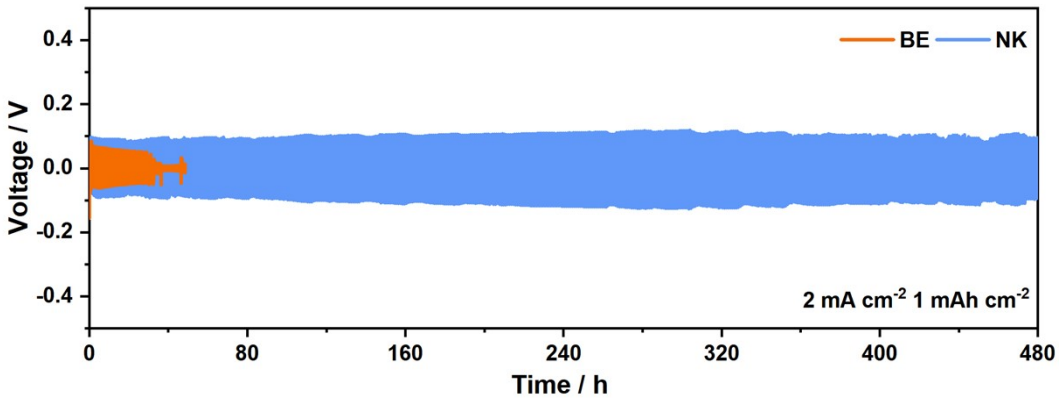

Fig S13 Cycling performance of symmetric batteries at 2 mA cm^{-2} and 1 mAh cm^{-2}.

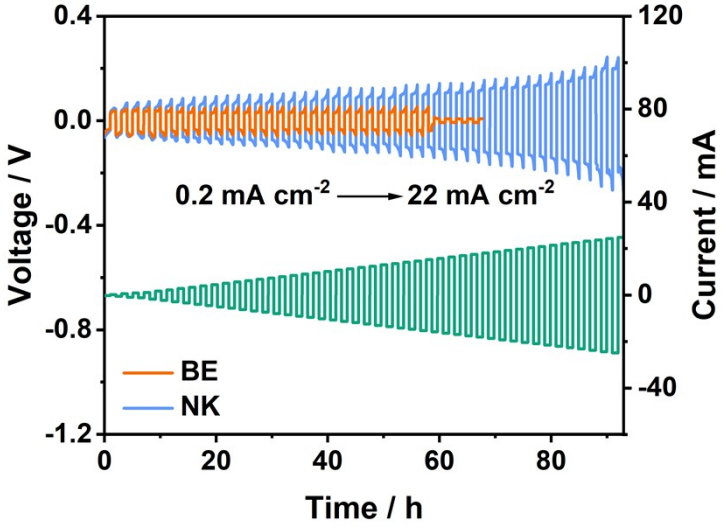

Fig. S14 Critical current density (CCD) test for symmetrical batteries.

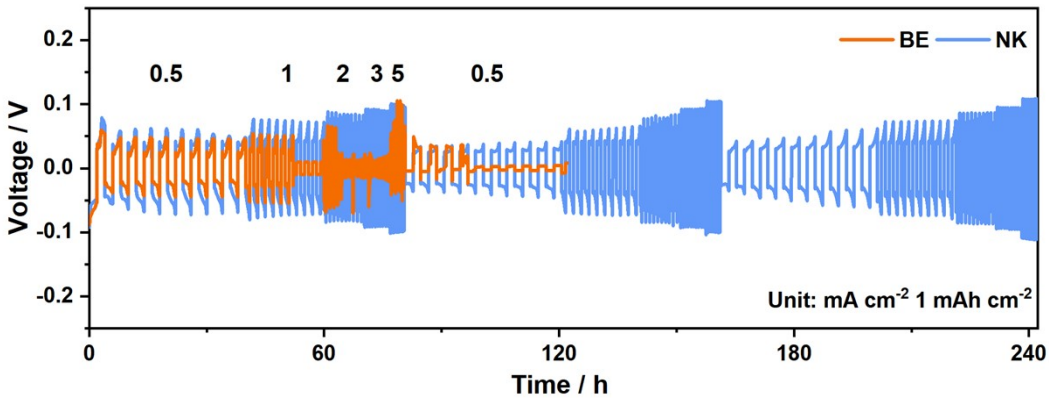

Fig. S15 Rate performance of symmetric batteries at different current densities from 0.5 to 5 mA cm^{-2}.

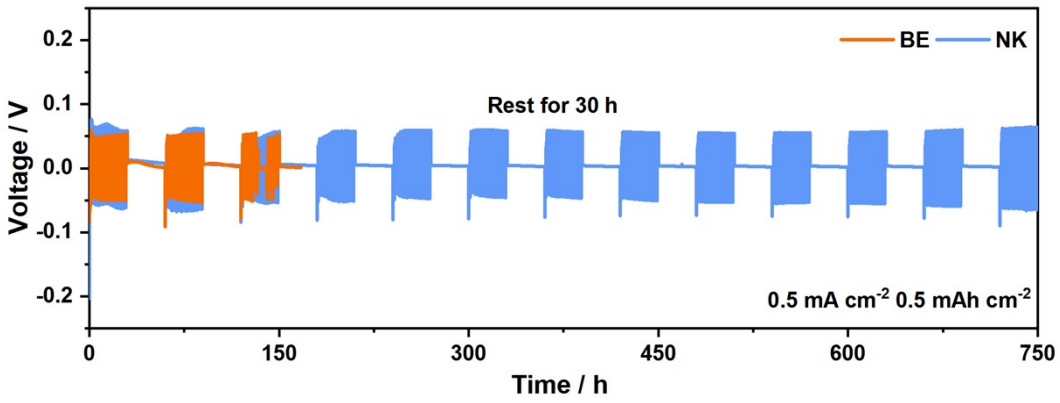

Fig. S16 Shelving-recovery performance of symmetric batteries.

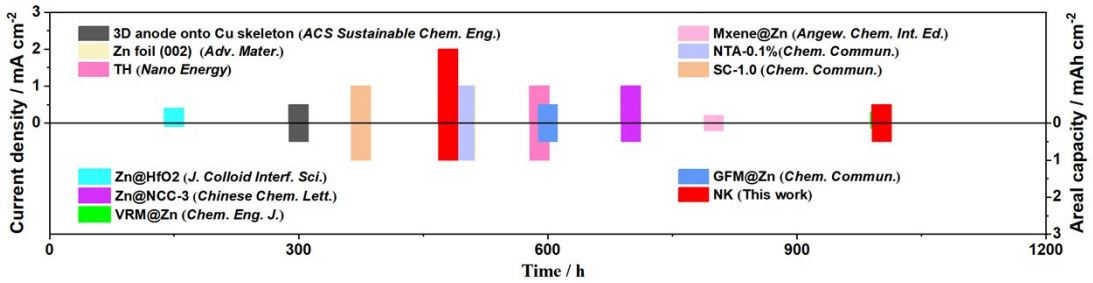

Fig. S17 Comparison of symmetric batteries performance with previous works.

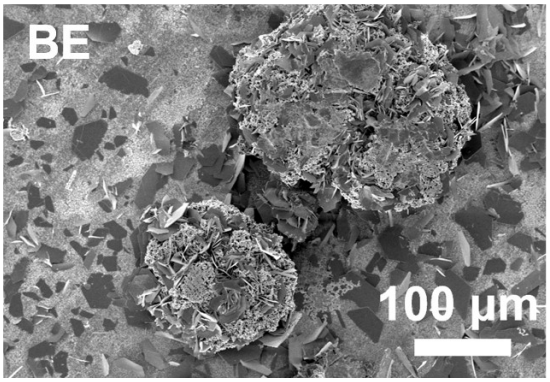

Fig. S18 SEM images of the zinc anode after 50 cycles in BE electrolyte.

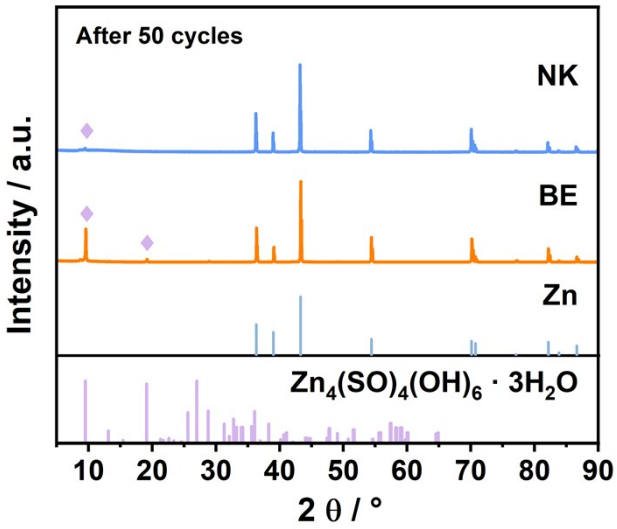

Fig. S19 XRD pattern of zinc surface after 50 cycles at the current density of 0.5 mA cm^{-2} in the battery assembled with different electrolytes.

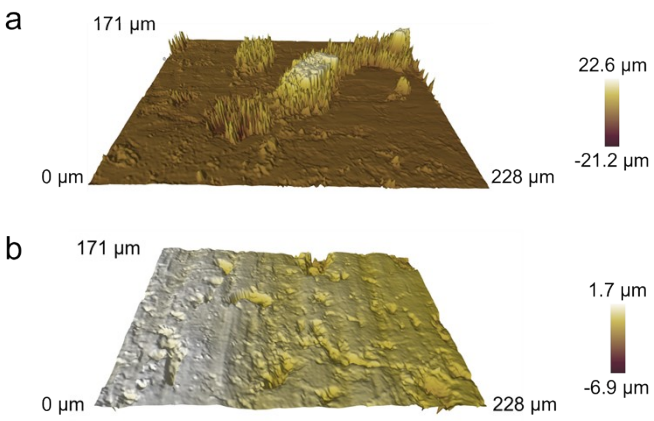

Fig. S20 Optical surface profilometry images of the zinc anode surface assembled with (a) BE and (b) NK electrolytes after 50 cycles at 0.5 mA cm^{-2}.

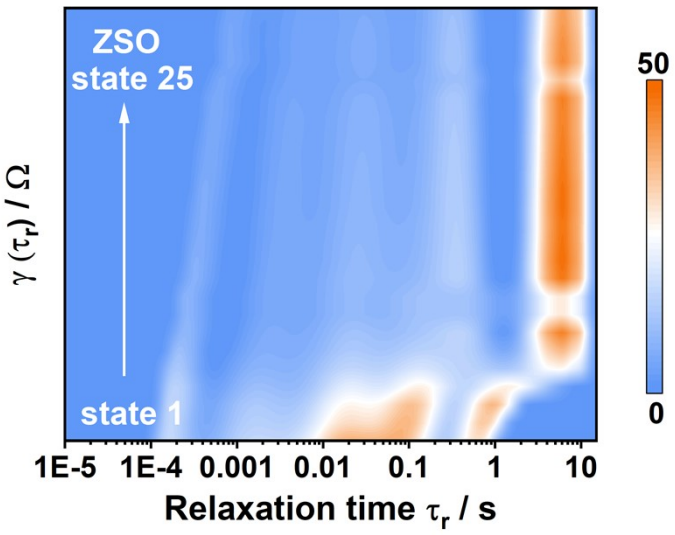

Fig. S21 DRT evolution of the symmetric battery assembled with the NK electrolyte during the zinc deposition process.

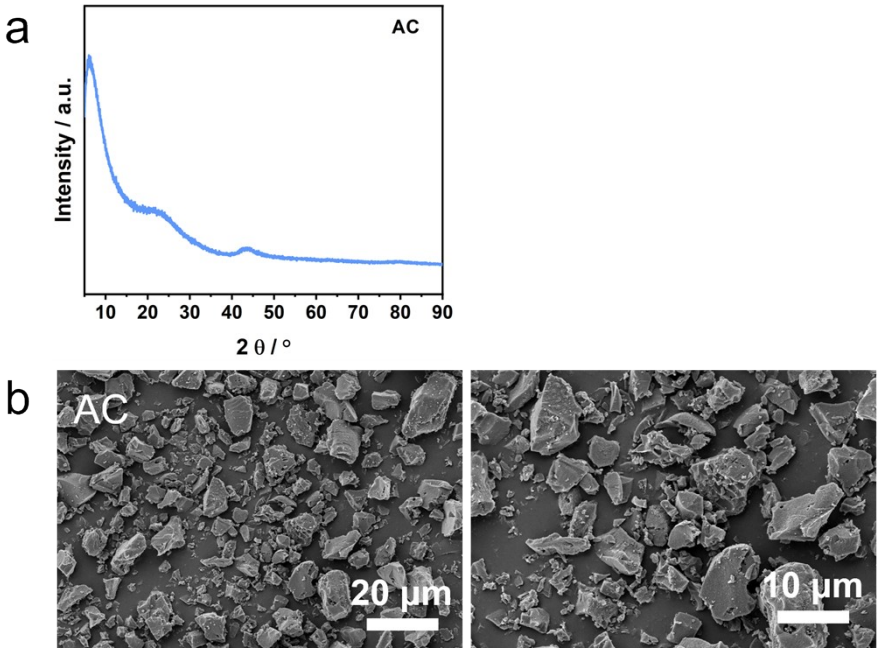

Fig. S22 (a) XRD pattern and (b) SEM images of AC.

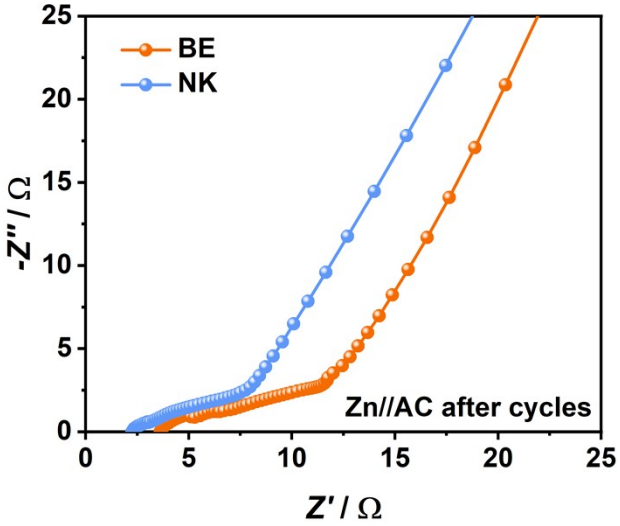

Fig. S23 EIS of ZICs utilizing BE and NK electrolytes after cycles.

Table S1 Comparison of cycle life performance between this work and the previously

Strategy	Current Density (mA cm^{-2})	Areal Capacity (mAh cm^{-2})	Cycle Time (hour)	Reference
3D anode onto Cu skeleton	0.5	0.5	300	[1]
Zn foil (002)	1	1	500	[2]
TH	1	1	590	[3]
Zn@HfO_2	0.4	0.1	150	[4]
Zn@NCC-3	1	0.5	700	[5]
VRM@Zn	0.3	0.15	1000	[6]
Mxene@Zn	0.2	0.2	800	[7]
NTA-0.1%	1	1	500	[8]
SC-1.0	1	1	375	[9]
GFM@Zn	0.5	0.5	600	[10]
Tish work	**0.5**	**0.5**	**1000**	
	2	**1**	**480**	

works.

Reference:

1. Z. Kang, C. Wu, L. Dong, W. Liu, J. Mou, J. Zhang, Z. Chang, B. Jiang, G. Wang, F. Kang and C. Xu, *ACS Sustainable Chem. Eng.*, 2019, **7**, 3364.
2. M. Zhou, S. Guo, J. Li, X. Luo, Z. Liu, T. Zhang, X. Cao, M. Long, B. Lu, A. Pan, G. Fang, J. Zhou and S. Liang, *Adv. Mater.*, 2021, **33**, 2100187.
3. Z. Miao, Q. Liu, W. Wei, X. Zhao, M. Du, H. Li, F. Zhang, M. Hao, Z. Cui, Y. Sang, X. Wang, H. Liu and S. Wang, *Nano Energy*, 2022, **97**, 107145.
4. B. Li, J. Xue, C. Han, N. Liu, K. Ma, R. Zhang, X. Wu, L. Dai, L. Wang and Z. He, *J. Colloid Interf. Sci.*, 2021, **599**, 467.
5. L. Wang, G. Fan, J. Liu, L. Zhang, M. Yu, Z. Yan and F. Cheng, *Chinese Chem. Lett.*, 2021, **32**, 1095.
6. B. Zhou, A. Hu, X. Zeng, M. He, R. Li, C. Zhao, Z. Yan, Y. Pan, J. Chen, Y. Fan, M. Liu and J. Long, *Chem. Eng. J.*, 2022, **450**, 137921.
7. N. Zhang, S. Huang, Z. Yuan, J. Zhu, Z. Zhao and Z. Niu, *Angew. Chem. Int. Ed.*, 2021, **60**, 2861.
8. H. Wang, Y. Su, L. Yan, X. Zeng, X. Chen, B. Xiang, H. Ren, T. Ma and M. Ling, *Chem. Commun.*, 2023, **59**, 11847.
9. C. Chen, L. Li, Z. Long and Q. Liang, *Chem. Commun.*, 2023, **59**, 13363-13366.
10. S. Liao, T. Shu, X. Yang, H. Li, X. Ma, Z. Liu, Y. Zhang and K. X. Yao, *Chem. Commun.*, 2024, **60**, 8928.